Title: Size-Dependence of Zirconia-based Ceramics via Deformation Twinning

Authors: H. Zhang[1]*, H. Gu[2], J. Jetter[3], E. Quandt[3], R. D. James[2], J. R. Greer[1].

Affiliations:

[1]Division of Engineering and Applied Science, California Institute of Technology, Pasadena, CA 91125, United States.

[2]Department of Aerospace Engineering and Mechanics, University of Minnesota, Minneapolis, MN 55455, USA.

[3]Institute for Material Science, Faculty of Engineering, University of Kiel, Kaiserstr. 2, 24143 Kiel, Germany.

*Correspondence to: hzhang3@caltech.edu

Abstract: Contrary to the dislocation-driven 'smaller-is-stronger' size-effect in nanocrystals, the size-dependence of strength in deformation twinning, another carrier of plasticity, still lacks universal understanding. Deformation twinning enables pseudoplastic strain of >5% in a shape memory ceramic $(ZrHfO_4)_x(YTaO_4)_{1-x}$. We use diffraction methods, microstructure analysis, and in-situ nanomechanical experiments to uncover contributing factors to the competition between twinning and slip in these submicron-sized ionic crystals, revealing power-law scaling of strength with size for both mechanisms. The significant twinning size-dependence was found to follow a superimposed power-law with exponent of -1, identical to that in metals. These findings unveil the universality of the superimposed power-law size-effect for twinning in single-crystals and provide new insights on deformability of ceramics and microstructure-driven nano-plasticity.

One Sentence Summary: Twinning-induced large deformation in single-crystal ceramics with significant size-effect on strength.

Main Text: Permanent deformation of single-crystalline materials, like metals and ceramics, can occur via two distinct plasticity carriers at room temperature: dislocation slip and deformation twinning. Over the past two decades, the widely-adopted power-law scaling of yield point with crystal size, with a universal exponent of -0.6 in fcc metals (*1–3*), was extended to metals with lower symmetry and/or higher internal friction (*4, 5*), as well as to hard-brittle materials such as ionic (*6*) or covalent crystals (*7*), where the power-law coefficient was suppressed to under -0.3. The inverse correlation between power-law exponent and internal lattice friction (*8, 9*) confronts the universality of the pure power-law, prompting the superimposed power-law function for the yield-point size-dependence, $\tau_c = a^{-1} + \tau_0$, where τ_c is the critical shear stress, a is the normalized sample size, and τ_0 is the size-independent bulk yield strength that depends purely on internal lattice friction and initial dislocation density (*6*). Unlike the varying exponents in numerous reported power-law scaling for different single crystals, the proposed inverse relation with a fixed exponent of -1 allows for a concrete physical interpretation under, for example, the well-defined Matthews-Blakeslee critical thickness model (*10*). The statistical analysis for such models become ambiguous at larger sample sizes, where plasticity shifts into a dislocation-interaction-dominated regime, giving rise to strengthening mechanisms (*10–12*) and thus preventing accurate estimates for the corresponding bulk strength. The limited size range in which the -1 exponent remains dominant has become a pervasive roadblock to an unambiguous observation of the -1 exponent in single-crystalline plasticity (*13*).

Despite controversy around the pure power-law with varying coefficients (*6*, *13*, *14*), it remains popular for the characterization of deformation mechanisms, including twinning, outside the realm of dislocation slip (*15–17*). The only superimposed power-law with exponent of -1 for single-crystal twinning was experimentally observed in Ti nanopillars (*18*), where it was attributed to a stimulated slip model that is unique to coherent twinning. Deformation twinning, as was theorized and observed (*19*, *20*), is nucleated by a leading partial dislocation and a trailing one on a separate atomic plane, creating an extended stacking fault that becomes the initial stage of a twin band. As a result, twinning is commonly found in metals with low stacking fault energies (*21–23*) and in crystals with low symmetry (*24*, *25*), caused by the lack of accessible crystallographic planes for dislocation slip. With the twinning partials' glide restricted to parallel planes, the common mechanisms for Taylor hardening, i.e. dislocation entanglements, pinning, and multiplication (*11*), remain largely irrelevant, making it an ideal mechanism for probing the fixed -1 exponent. In addition to existing works on metals, it is necessary to study deformation twinning in hard brittle crystals, for example monoclinic zirconia, a common ionic ceramic that produces coherent twin domains upon phase-transformation (*26*, *27*) and can be adapted in composition to undergo >5% stress-induced twinning at room temperature (*28*).

We chose one compositional adaptation, $(ZrHfO_4)_{0.735}(YTaO_4)_{0.265}$ (hereafter referred to as $(ZrHfO_4)_{0.735}$), which was theoretically and experimentally found to produce the largest twinning-induced plastic strain and the smallest thermal transformation hysteresis (*28*, *29*). We uncover the twinning mechanism via site-specific systematic nanomechanical experiments and microstructural analysis, identify the conditions under which twinning is preferred over ordinary dislocation slip, and probe the overall size-dependence of the stress required for the nucleation of twinning. We discuss these findings in the framework of nano-plasticity in single-crystals to identify the universality of the extrinsic size-effect in deformation twinning.
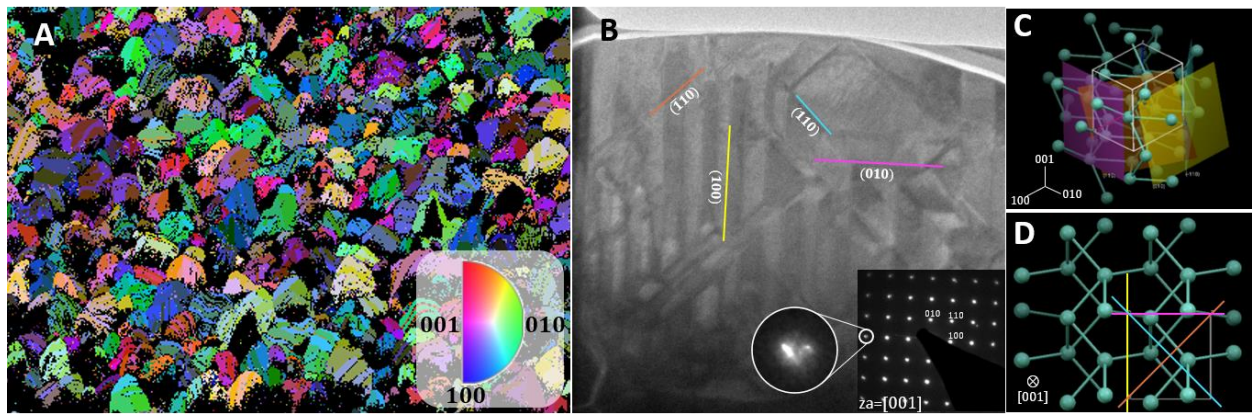
Results

Fig. 1. *Microstructure of $(ZrHfO_4)_{0.735}(YTaO_4)_{0.265}$. (A) An inverted pole EBSD map along the surface normal of randomly oriented monoclinic grains that contain nano-twins. Inset: IPF; the scale bar is 20μm. (B) TEM image of a typical grain that contains multiple twin boundaries mainly along the close-packed planes and twin domains whose widths range from 50nm to 500nm (28). The diffraction pattern (inset) obtained from the entire grain suggests that the twinning direction is oriented along the diffraction zone axis, [001], where the signature of twinning appears as separation of spots at high Miller indices caused by variations in the diffraction error. Scale bar is 500nm. Crystal structure of ZrO_2 (only Zr atoms are shown)*

viewed (C) in 3D and (D) from the TEM diffraction zone axis [001] direction, both including the observed mirror planes depicted with consistent colors as (B).

Sample crystallography and initial microstructure were analyzed through Electron Backscattering Diffraction (EBSD) and Transmission Electron Microscopy (TEM). Figure 1A shows the EBSD map of a polycrystalline puck, revealing randomly oriented, ~5µm-sized monoclinic grains. Single grain TEM uncovers shared [001] zone axis among multiple twin variants (Figure 1B), as evidenced by the splitting of diffraction spots at higher miller indices, such as the ($\bar{3}$00) triplet (Fig. 1B, zoomed-in inset) (28), with average twin width of 200nm. Mirror planes fall along the monoclinic close-packed planes of {100}, {010}, or {110} with high coherency (Figure S1), consistent with that reported for room-temperature zirconia (26). Figure 1C shows the observed mirror planes overlaid onto a monoclinic ZrO_2 lattice in 3D and Figure 1D shows them at the same viewing configuration as Figure 1B. The coherent mirror planes provide easily accessible deformation twinning systems of {100}⟨001⟩, {010}⟨001⟩, and {110}⟨001⟩ (20).
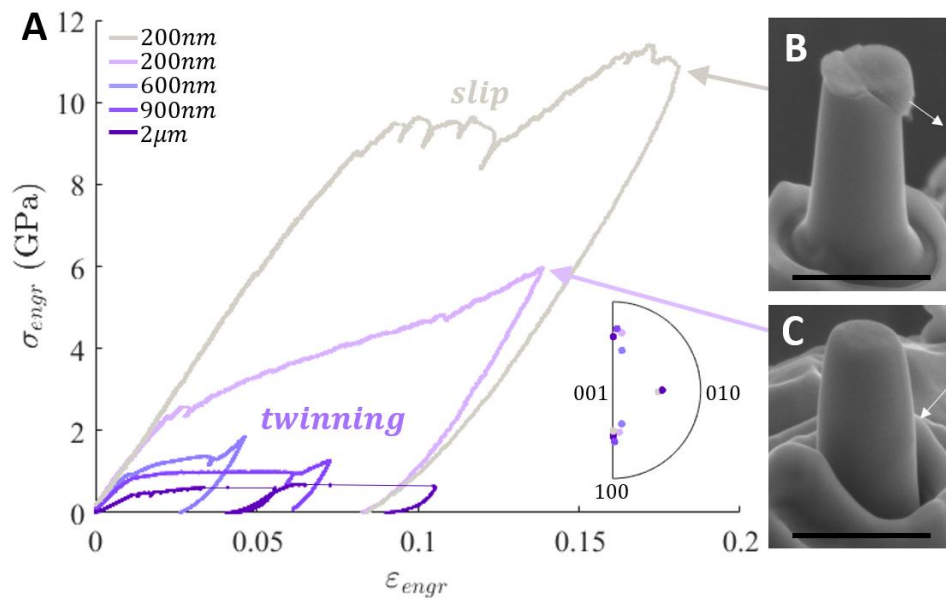

Fig. 2. (A) Representative engineering stress-strain data for pillars of different diameters fabricated from grains with similar orientations close to [101], [$\bar{1}$01], *and* [011] *that deformed via twinning (purple) and slip (grey). The inset IPF contains the exact orientations of each pillar's parent grain along the loading direction, identified through EBSD. Post compression SEM images of 200nm-diameter pillars that deformed via (B) slip and (C) twinning, with the slip/twinning directions indicated by white arrows. Scale bars are 500nm.*

Cylindrical pillars with diameters ranging from 200nm to 2µm were milled from $(ZrHfO_4)_{0.735}$ grains of different orientations (as identified from EBSD) using a top-down approach with a Ga+ Focused Ion Beam (FIB, see Supplemental Materials). Figure 2A shows representative uniaxial compression stress-strain data for pillars with roughly [101]/[$\bar{1}$01]/[011] parent grain orientations along the loading direction, corrected for substrate effects using Scanning Electron Microscope (SEM) image correlation (Figure S2). The exact loading orientations for each pillar are presented in the Inverted Pole Figure (IPF) (Figure 2A, inset), which favor the same twin system (100)[001]. Twinning was found to be the preferred deformation mechanism in this

orientation, with five out of seven 200nm diameter pillars and all eleven larger pillars deforming via twinning and only two 200nm pillars deforming via slip. The response of four typical pillars of different sizes that deformed via twinning is plotted in purple in Figure 2A. After the initial linear-elastic region, plasticity is triggered at a critical stress σ_c (defined as the stress before the first plasticity-induced stress-drop, Fig. S3) that decreases with size, followed by steady serrated plastic flow, which is a typical trait of deformation twinning (15, 30). As it takes higher stress to nucleate a twin than to propagate an existing twin boundary, twinning is induced by the growth of existing twins. While the flow stress stays stable for the two larger pillars, the two smaller pillars exhibit strain hardening as a result of the fabrication induced tapering (Figure S4). All sub-micron pillars deformed to >4% engineering strain without catastrophic failure, with the 200nm pillar compressing to 13% and retaining 8% plastic strain post-unloading, which is on par with that seen in ductile metals (15, 18, 19). Twinning without fracture was also found in samples up to ~5µm in size of non-standard shape (Figure S5). The mechanical response of a 200nm pillar that deformed via dislocation slip (grey) yields at a strain of 8% and a 4x higher stress, with subsequent stochastic strain bursts that are a signature of slip dislocation avalanches (1, 31). As the pillar size decreases to the average twin width of 200nm, the probability of it not containing a suitable orientation for twinning increases, in which case the pillar yields only when it reaches the much higher required stress for slip. Post-compression images of the 200nm pillars that deformed via slip (Figure 2B) exhibit shear offsets that are characteristic of dislocation slip at the nanoscale (2) with the slip direction marked by the white arrow. Samples that twinned (Figure 2C) undergo a reorientation-induced shear, with the white arrow marking the twin direction. Post-compression images of larger size pillars can be found in Figure S6.
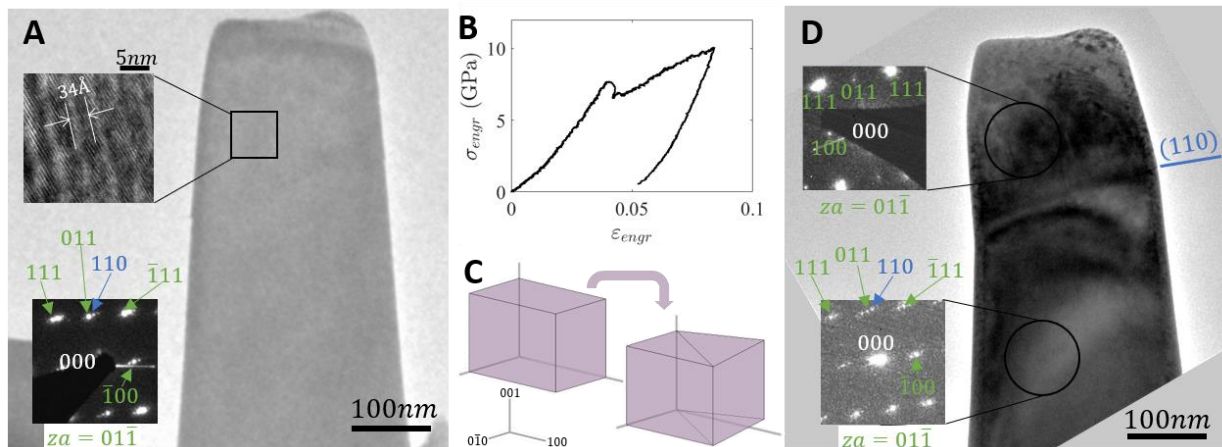
***Fig. 3.** (A) 100nm thick (ZrHfO₄)₀.₇₃₅ rectangular nano-pillar imaged in TEM, with 34Å-spaced Moiré fringes visible at high resolution (inset, top left); the diffraction pattern (inset, lower left) contains orientations with a* [011] *zone axis (green) and coherency spots generated by superposition of a separate orientation where only the* {110} *reflections are diffracting (blue). (B) Engineering stress-strain data for the compression of the shown pillar. (C) Crystallographic diagram of the* (110)[001] *twinning for a unit cell. (D) TEM image of the same pillar after compression, whose top region has permanently deformed via twinning and contains only the* [01$\bar{1}$] *orientation, with no Moiré character or diffraction spot splitting; the lower undeformed region of the pillar stays unchanged. The twinning plane is along the original blue* (110) *plane.*

TEM analysis was used to uncover deformation twinning by imaging a FIB-milled 100nm-thick nanopillar (see Supplemental Materials) both before and after *in-situ* SEM uniaxial compression. Figure 3A conveys the TEM image of the single-crystalline pillar as-fabricated, along with a high-resolution image (upper-left inset) that contains 34Å-spaced Moiré fringes which arise from stacking of two orientations identified in the diffraction pattern (DP, lower-left inset): one orientation along the [01$\bar{1}$] zone axis (green) and the other oriented favorably only for diffraction from (110) planes, resulting in the additional (110) dot (blue). The (110) planes on top of the existing [01$\bar{1}$] pattern produce satellite peaks whose intensity is sufficiently visible only in the vicinity of the diffraction spots (*32*), resulting in the triplet-like DP. The theoretical diffraction difference between the green (111) and blue (110) spots matches the predicted 0.029Å^{-1} from the measured Moiré spacing. The pillar was then uniaxially compressed in the SEM, with the engineering stress-strain data shown in Figure 3B, revealing elastic loading up to 3.5% strain, followed by a sudden 10% stress drop after onset of deformation twinning at $\sigma_c =$ 8GPa. The pillar then steadily hardens with a ~75GPa slope while the twin plane migrates downwards at increasing cross-sectional area to 8% engineering strain with 5% plastic strain. A crystallographic diagram of the twinning system is presented in Figure 3C, where the monoclinic unit cell shears along the (110) plane in the [001] direction. Figure 3D shows the post-compression TEM image, where the top portion of the pillar has undergone coherent shearing, a signature of deformation twinning (*18, 21*). This twinning-induced reorientation eliminates the Moiré pattern, leaving solely the [01$\bar{1}$] DP (upper-left inset), while the lower undeformed section contains the original crystal orientations with the Moiré character. The disappearance of (110) spots and the observed (110) twin plane confirms the (110)[001] twinning system.
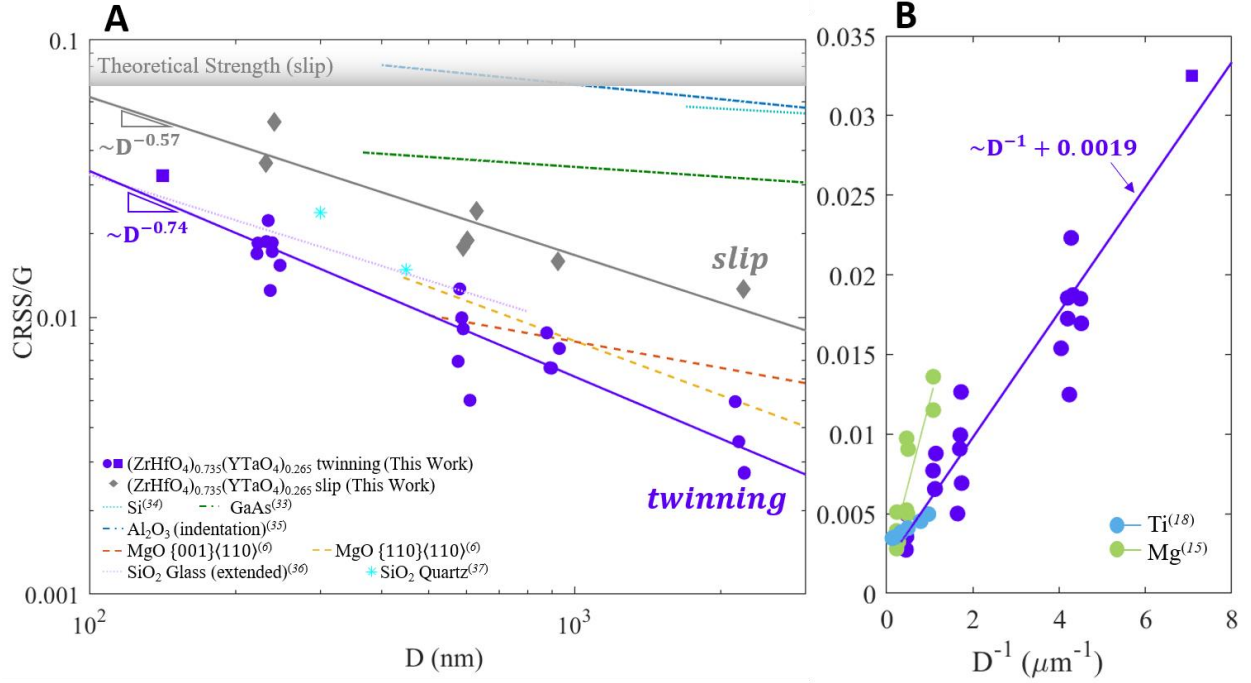
Discussion

Fig. 4. *(A) Normalized CRSS as a function of effective pillar diameter for two sets of orientations, with opposite preferred deformation mechanism, in the (ZrHfO₄)₀.₇₃₅ system with the corresponding power-law fit to guide the eye, in comparison to other ceramics (6, 33–37). The CRSS required for twinning is lowest among all and its size-effect most prominent. (B) Twinning (ZrHfO₄)₀.₇₃₅ pillars fitted with the superimposed power-law (Eq. 3) resulting in $\alpha = 1 \pm 0.22$, in comparison to that found in Ti (18) and Mg (15), both scaling inversely with D.*

Despite twinning being the preferred plasticity carrier in (ZrHfO₄)₀.₇₃₅, it is possible to dislocation slip in larger pillars by aligning the loading direction to the twinning direction [001], which results in negligible resolved shear stress on all three twin planes. We investigated the critical resolved shear stress (CRSS) for both slip and twinning, calculated using Eq. 1, as a function of the characteristic pillar diameter.

$$CRSS = \sigma_c s = \sigma_c(\boldsymbol{n}_{load} \cdot \hat{\boldsymbol{n}}_{twin})(\boldsymbol{n}_{load} \cdot \boldsymbol{\lambda}_{twin}). \tag{Eq. 1}$$

Here, s is the maximum Schmid factor among combinations of pillar orientations and accessible twin/slip systems; $\boldsymbol{n}_{load}$ is the loading direction, $\hat{\boldsymbol{n}}_{twin}$ is the twin/slip plane normal, and $\boldsymbol{\lambda}_{twin}$ is the twin/slip direction. Figure 4A plots normalized CRSS vs. *D* for both twinning (purple) and slip (gray) orientations. The shear modulus, $G = 61.5 GPa$, was estimated from the linear unloading segments in 200nm pillars, consistent with previous reports on Yttrium-stabilized Zirconia (*38*, *39*). The spread of measured yield stress at fixed pillar size is common for nanopillar compression as a result of imperfect alignment, machine compliance, and stochastic plastic events. (*1–4*, *6*, *8*). Starting with the widely adopted pure power-law (fitted with least-square regression)

$$CRSS \propto D^{-\alpha}, \tag{Eq. 2}$$

the twinning exponent of 0.74 ± 0.10, found to be universal among different orientations and compositions (Figure S7), is higher than the 0.57 ± 0.22 for slip and that for other brittle materials (dashed lines) (*33–36*) deforming through slip or fracture; this work presents the first known systematic size-effect for twinning in a non-metallic material. This large increase of size-dependence from slip to twinning finds its equivalence in metals, where a similar exponent of $\alpha = 0.7$ was discovered for twinning in Mg (*15*), and an unprecedented $\alpha = 1$ for Ti (*18*). Previous report on deformation twinning in another oxide, quartz, (*37*) (teal stars) show emergence of a similar trend, although no conclusion was drawn due to the small size span.

For a macroscopically brittle material, the size-effect for materials with high background stress is more properly represented as

$$CRSS = \xi D^{-\alpha} + \tau_0. \tag{Eq. 3}$$

ξ is a length-scale constant that scales with the Burgers' vector and τ_0 is the resolved macroscale yield strength. Fitting Eq. 3 to the twinning data (see Supplemental Materials) for $(ZrHfO_4)_{0.735}$ results in $\alpha = 1.00 \pm 0.22$ and $\tau_0/G = 0.0019 \pm 0.0018$ (Figure 4B), with the average α identical to that predicted by the Matthews-Blakeslee critical thickness model, which emerges as equilibrium is reached between the plastic strain and the curvature of geometrically-necessary (misfit) dislocations (*10*). The fitted result is compared to that observed in metals. The size-dependence of twinning in Ti (*18*) exhibits the identical form as Eq. 3 with -1 exponent, but was theorized as a Hall-Petch type relationship with the critical dislocation density for twinning scaling as D^2. We fit previously reported Mg *CRSS* (*15*) to Eq. 3, only including data between 1μm and 5μm since smaller pillars plateau at theoretical strength, resulting in $\alpha = 1.00 \pm 0.38$ and bulk strength $\tau_0/G = 0.0017 \pm 0.0034$; this estimated τ_0 is close to that reported for mm-size Mg samples (*40*). The uncanny similarities among the drastically different systems in Figure 4B suggest universality of Eq. 3 with fixed $\alpha = 1$ for a larger selection of materials.

Conclusion

Deformation twinning in single-crystals and its dependence on extrinsic dimensions has not been fully understood at the nanoscale. In this work we uncover twinning as the preferred plasticity carrier for small volume $(ZrHfO_4)_{0.735}(YTaO_4)_{0.265}$ ceramics, while dislocation slip can be activated only when no accessible orientation for twinning exists. In the sub-micron range, these single-crystal oxides plastically deform up to 10% strain through twinning without failure. While the power-law exponent for the yield stress size-effect of slip is close to that in fcc metals, we reveal the first systematic strength-to-size dependence for twinning in ceramics. This significant size-effect was found to follow the inverse-like relationship with exponent $\alpha = 1$ when considering a superimposed bulk strength, identical to the twinning size-effect in soft metallic materials. The large similarities between a brittle oxide and ductile metals shed light on the universality of the Matthews-Blakeslee critical thickness model for the yield-point size-effect in single-crystal plasticity, suggesting deformation twinning as an alternative controllable way of probing its exact physical origin.

References and Notes:

1. M. D. Uchic, D. M. Dimiduk, J. N. Florando, W. D. Nix, Sample dimensions influence strength and crystal plasticity. *Science (80-.).* **305**, 986–989 (2004).

2. J. R. Greer, W. C. Oliver, W. D. Nix, Size dependence of mechanical properties of gold at

the micron scale in the absence of strain gradients. *Acta Mater.* **53**, 1821–1830 (2005).

3. A. T. Jennings, M. J. Burek, J. R. Greer, Microstructure versus Size: Mechanical properties of electroplated single crystalline Cu nanopillars. *Phys. Rev. Lett.* **104**, 1–4 (2010).

4. J. Y. Kim, D. Jang, J. R. Greer, Tensile and compressive behavior of tungsten, molybdenum, tantalum and niobium at the nanoscale. *Acta Mater.* **58**, 2355–2363 (2010).

5. J. Ye, R. K. Mishra, A. K. Sachdev, A. M. Minor, In situ TEM compression testing of Mg and Mg-0.2 wt.% Ce single crystals. *Scr. Mater.* **64**, 292–295 (2011).

6. S. Korte, W. J. Clegg, Discussion of the dependence of the effect of size on the yield stress in hard materials studied by microcompression of MgO. *Philos. Mag.* **91**, 1150–1162 (2011).

7. F. Östlund, K. Rzepiejewska-Malyska, K. Leifer, L. M. Hale, Y. Tang, R. Ballarini, W. W. Gerberich, J. Michler, Brittle-to-ductile transition in uniaxial compression of silicon pillars at room temperature. *Adv. Funct. Mater.* **19**, 2439–2444 (2009).

8. J. R. Greer, J. T. M. De Hosson, Plasticity in small-sized metallic systems: Intrinsic versus extrinsic size effect. *Prog. Mater. Sci.* **56**, 654–724 (2011).

9. A. S. Schneider, D. Kaufmann, B. G. Clark, C. P. Frick, P. A. Gruber, R. Mönig, O. Kraft, E. Arzt, Correlation between critical temperature and strength of small-scale bcc pillars. *Phys. Rev. Lett.* **103**, 105501 (2009).

10. J. W. Matthews, A. E. Blakeslee, Defects in epitaxial multilayers: I. Misfit dislocations. *J. Cryst. Growth*. **27**, 118–125 (1974).

11. S. I. Rao, D. M. Dimiduk, T. A. Parthasarathy, M. D. Uchic, M. Tang, C. Woodward, Athermal mechanisms of size-dependent crystal flow gleaned from three-dimensional discrete dislocation simulations. *Acta Mater.* **56**, 3245–3259 (2008).

12. J. A. El-Awady, C. Woodward, D. M. Dimiduk, N. M. Ghoniem, Effects of focused ion beam induced damage on the plasticity of micropillars. *Phys. Rev. B - Condens. Matter Mater. Phys.* **80**, 1–5 (2009).

13. D. J. Dunstan, A. J. Bushby, The scaling exponent in the size effect of small scale plastic deformation. *Int. J. Plast.* **40**, 152–162 (2013).

14. D. J. Dunstan, The size effect in the mechanical strength of semiconductors and metals: Strain relaxation by dislocation-mediated plastic deformation. *J. Mater. Res.* **32**, 4041–4053 (2017).

15. J. Jeong, M. Alfreider, R. Konetschnik, D. Kiener, S. H. Oh, In-situ TEM observation of {101¯2} twin-dominated deformation of Mg pillars: Twinning mechanism, size effects and rate dependency. *Acta Mater.* **158**, 407–421 (2018).

16. I. Basu, V. Ocelík, J. T. M. De Hosson, Size effects on plasticity in high-entropy alloys. *J. Mater. Res.* **33**, 3055–3076 (2018).

17. G. D. Sim, G. Kim, S. Lavenstein, M. H. Hamza, H. Fan, J. A. El-Awady, Anomalous hardening in magnesium driven by a size-dependent transition in deformation modes. *Acta Mater.* **144**, 11–20 (2018).

18. Q. Yu, Z. W. Shan, J. Li, X. Huang, L. Xiao, J. Sun, E. Ma, Strong crystal size effect on deformation twinning. *Nature*. **463**, 335–338 (2010).

19. J. Wang, Z. Zeng, C. R. Weinberger, Z. Zhang, T. Zhu, S. X. Mao, In situ atomic-scale observation of twinning-dominated deformation in nanoscale body-centred cubic tungsten. *Nat. Mater.* **14**, 594–600 (2015).

20. X. Li, Y. Wei, L. Lu, K. Lu, H. Gao, Dislocation nucleation governed softening and maximum strength in nano-twinned metals. *Nature*. **464**, 877–880 (2010).

21. S. Lee, J. Im, Y. Yoo, E. Bitzek, D. Kiener, G. Richter, B. Kim, S. H. Oh, Reversible cyclic deformation mechanism of gold nanowires by twinning-detwinning transition evidenced from in situ TEM. *Nat. Commun.* **5**, 1–10 (2014).

22. X. Z. Liao, Y. H. Zhao, S. G. Srinivasan, Y. T. Zhu, R. Z. Valiev, D. V. Gunderov, Deformation twinning in nanocrystalline copper at room temperature and low strain rate. *Appl. Phys. Lett.* **84**, 592 (2004).

23. K. Lu, L. Lu, S. Suresh, Strengthening materials by engineering coherent internal boundaries at the nanoscale. *Science (80-.).* **324**, 349–352 (2009).

24. D. W. Brown, S. R. Agnew, M. A. M. Bourke, T. M. Holden, S. C. Vogel, C. N. Tomé, Internal strain and texture evolution during deformation twinning in magnesium. *Mater. Sci. Eng. A*. **399**, 1–12 (2005).

25. T. Ezaz, H. Sehitoglu, Type II detwinning in NiTi. *Appl. Phys. Lett.* **98**, 3–5 (2011).

26. E. Bischoff, M. Ruhle, Twin Boundaries in Monoclinic ZrO2 Particles Confined in a Mullite Matrix. *J. Am. Ceram. Soc.* **66**, 123–127 (1982).

27. J. Chevalier, L. Gremillard, A. V. Virkar, D. R. Clarke, The tetragonal-monoclinic transformation in zirconia: Lessons learned and future trends. *J. Am. Ceram. Soc.* **92**, 1901–1920 (2009).

28. J. Jetter, H. Gu, H. Zhang, M. Wuttig, X. Chen, J. R. Greer, R. D. James, E. Quandt, Tuning crystallographic compatibility to enhance shape memory in ceramics. *Phys. Rev. Mater.* **3**, 093603 (2019).

29. X. Chen, V. Srivastava, V. Dabade, R. D. James, Study of the cofactor conditions: Conditions of supercompatibility between phases. *J. Mech. Phys. Solids*. **61**, 2566–2587 (2013).

30. S. Miyazaki, K. Otsuka, Y. Suzuki, Transformation pseudoelasticity in NiTi. *Scr. Metall.* **15**, 287–292 (1981).

31. F. F. Csikor, C. Motz, D. Weygand, M. Zaiser, S. Zapperi, Dislocation avalanches, strain bursts, and the problem of plastic forming at the micrometer scale. *Science (80-.).* **318**, 251–254 (2007).

32. B. Fultz, J. Howe, *Transmission Electron Microscopy and Diffractometry of Materials* (Springer, ed. 4, 2013).

33. F. Östlund, P. R. Howie, R. Ghisleni, S. Korte, K. Leifer, W. J. Clegg, J. Michler, Ductile-brittle transition in micropillar compression of GaAs at room temperature. *Philos. Mag.* **91**, 1190–1199 (2011).

34. B. Moser, K. Wasmer, L. Barbieri, J. Michler, Strength and fracture of Si micropillars: A new scanning electron microscopy-based micro-compression test. *J. Mater. Res.* **22**, 1004–1011 (2007).

35. T. T. Zhu, A. J. Bushby, D. J. Dunstan, Size effect in the initiation of plasticity for ceramics in nanoindentation. *J. Mech. Phys. Solids*. **56**, 1170–1185 (2008).

36. J. Luo, J. Wang, E. Bitzek, J. Y. Huang, H. Zheng, L. Tong, Q. Yang, J. Li, S. X. Mao, Size-Dependent Brittle-to-Ductile Transition in Silica Glass Nanofibers. *Nano Lett.* **16**, 105–113 (2016).

37. E. Tochigi, E. Zepeda-alarcon, H. R. Wenk, A. M. Minor, In situ TEM observations of plastic deformation in quartz crystals. *Phys. Chem. Miner.* **41**, 757–765 (2014).

38. J. Eichler, U. Eisele, J. Rödel, Mechanical properties of monoclinic zirconia. *J. Am. Ceram. Soc.* **87**, 1401–1403 (2004).

39. Z. Du, X. M. Zeng, Q. Liu, C. A. Schuh, C. L. Gan, Superelasticity in micro-scale shape memory ceramic particles. *Acta Mater.* **123**, 255–263 (2017).

40. K. Fukuda, Y. Koyanagi, M. Tsushida, H. Kitahara, T. Mayama, S. Ando, Activation stress for slip systems of pure magnesium single crystals in pure shear test. *Mater. Trans.* **58**, 587–591 (2017).

Acknowledgments:

Supplementary Materials:

Materials and Methods

Figures S1-S7